Liu, X., Du, B., Sun, Y., Yu, M., Yin, Y., Tang, W., Chen, C., Sun, L., Yang, B., Cao, W., & Ashfold, M. N. R. (2016). Sensitive Room Temperature Photoluminescence-Based Sensing of H2S with Novel CuO–ZnO Nanorods. *ACS Applied Materials and Interfaces*, *8*(25), 16379–16385. https://doi.org/10.1021/acsami.6b02455

Sensitive Room Temperature Photoluminescence-based Sensing of H_2S with Novel CuO-ZnO Nanorods

Xiao Liu,[†] *Baosheng Du,*[†] *Ye Sun,*[*,†] *Miao Yu,*[*,‡] *Yongqi Yin,*[†] *Wei Tang,*[†] *Chong Chen,*[‡] *Lei Sun,*[‡] *Bin Yang,*[†] *Wenwu Cao,*[†,§] *and Michael N. R. Ashfold*[*,∥]

[†] *Condensed Matter Science and Technology Institute, School of Science, Harbin Institute of Technology, Harbin 150080, China*

[‡] *State Key Laboratory of Urban Water Resource and Environment, School of Chemical Engineering and Technology, Harbin Institute of Technology, Harbin 150001, China*

[§] *Department of Mathematics and Materials Research Institute, The Pennsylvania State University, University Park, Pennsylvania16802, USA*

[∥] *School of Chemistry, University of Bristol, Bristol BS8 1TS, U.K.*

KEYWORDS: Cu-doped ZnO nanorods • heterostructure • pulsed laser deposition • vapour-solid-solid mode • gas sensing • optical sensor

ABSTRACT

Novel CuO nanoparticle-capped ZnO nanorods have been produced using a pulsed laser deposition (PLD) method. These nanorods are shown to grow by a CuO-nanoparticle-assisted vapour-solid-solid (V-S-S) mechanism. The photoluminescence (PL) accompanying ultraviolet illumination of these capped nanorod samples shows large variations upon exposure to trace quantities of H_2S gas. The present data suggests that both the Cu-doped ZnO stem and the CuO capping nanoparticle contribute to optical H_2S sensing with these CuO-ZnO nanorods. This study represents the first demonstration of PL-based H_2S gas sensing, at room temperature, with sub-ppm sensitivity. It also opens the way to producing CuO-ZnO nanorods by a V-S-S mechanism using gas phase methods other than PLD.

1. INTRODUCTION

Hydrogen sulfide (H_2S), a highly toxic, flammable and colorless gas, is widely found in petroleum refining, natural gas processing, coal mining and in the generation of biogas from bio-waste. Even short (10 min) exposures to H_2S, at concentrations as low as 15 ppm, can endanger human life. Inevitably, therefore, high-performance sensing of H_2S has become an important topic in recent years.[1-4] High sensitivities, down to ppm and even sub-ppm levels, have been demonstrated using a range of semiconducting metal oxides (e.g. ZnO,[5,6] CuO,[7] WO_3,[2] Cu_2O,[3,8] SnO_2,[9] and Fe_2O_3[10]). High sensitivity is just one of the important considerations with any sensor, however; the working temperature (T_w) is another. T_w for most reported H_2S gas sensors is in the range of 150-450 °C, [1-7,9,10] but room temperature (RT) sensing would be preferable from the perspectives of device fabrication, miniaturization, operation and safety, given the autoignition of H_2S at 260 °C in ambient atmosphere.[11-13]

Various strategies have been adopted to enhance H_2S sensing using metal oxides. These include doping, hetero-junctions and surface modifications, such as Cu-doped SnO_2 films,[14] Sb-doped SnO_2 nanoribbons,[15] Mo-doped ZnO nanowires,[16] CuO-SnO_2 nanowires,[17] Au surface-modified ZnO nanowires,[12] ZnS decorated ZnO nanorods (NRs) [18] and SnO_2@Ag nanostructures.[19] CuO-ZnO heterostructures and Cu-doped ZnO have attracted particular attention.[4,13,20-23] H_2S detection sensitivities in the 1-10 ppm range were demonstrated in most cases,[4,13,20-22] with higher (sub-ppm) sensitivity reported at high T_w.[23] Quite apart from the sensitivity, the low cost and high stability of both *n*-type ZnO and *p*-type CuO are also attractive features from the perspective of practical application.

However, all of the above are examples of electrical H_2S sensors. Optical sensors offer further potential benefits, including simplicity of device fabrication, and the fact that they can be operated remotely and in the presence of strong electromagnetic fields.[24-27] One of the many fascinating characteristics of ZnO materials is their distinctive photoluminescence (PL) under ultraviolet (UV) illumination, and optical sensing of oxygen,[25,28] nitrogen dioxide [29] and nitroaromatic derivatives [30] has been demonstrated by their effect on this PL. As noted above, PL-based gas sensors offer a significant potential advantage: the as-grown products can be used for optical gas sensing without the need for any electrical contact. However, to the best of our knowledge, no PL-based H_2S sensors have been reported prior to the present work.

Pulsed laser deposition (PLD) is a widely used method for producing high-quality pure (and doped) ZnO nanomaterials.[31-34] Our earlier works revealed both vapour-solid (V-S) and vapour-liquid-solid (V-L-S) modes of growing ZnO NRs by PLD, and realized controllable growth of both pure and Al-doped ZnO nanomaterials.[32,35-37] PLD NRs produced in this way were shown to offer a PL-based based route to sensing O_2 (at $T_w \geq 150$ °C).[25] However, we have not found any prior reports of the growth of ZnO-CuO heterostructured NRs or Cu-doped ZnO NRs by PLD methods.

The present work reports the growth (by PLD) of unique CuO nanoparticle-capped ZnO NRs, and provides insights into their likely vapour-solid-solid (V-S-S) formation mechanism (shown in left side of Scheme 1). Additionally, we explore the utility of these CuO-ZnO NRs as PL-based sensors, their selectivity and sensitivity to H_2S detection, demonstrate sub-ppm sensitivities for H_2S in ambient air even when operating at RT, and

attribute likely sensing mechanisms to Cu doping of the ZnO stems and the capping CuO nanoparticles (illustrated in right side of Scheme 1).

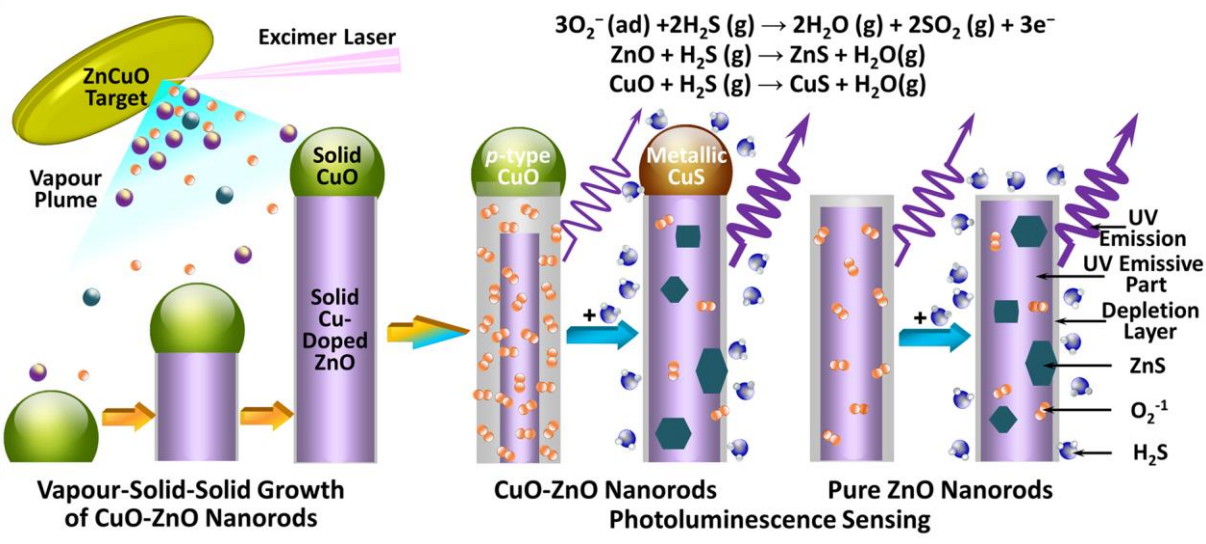

SCHEME 1. Schematic diagram illustrating (left) vapour-solid-solid growth of CuO-ZnO NRs and (right) H_2S gas sensing mechanisms with CuO-ZnO NRs and pure ZnO NRs.

2. EXPERIMENTAL SECTION

The CuO-ZnO NRs were produced on Si(100) substrates by PLD, using a KrF excimer laser (Lambda-Physik COMPex 205, λ = 248 nm, pulse duration of 25 ns, repetition rate of 8 Hz, and incident fluence ≈1.5 J cm^{-2}). The ceramic ZnCuO target (with Zn:Cu atomic ratio of 9:1) was rotated throughout the deposition, and the target-substrate separation was set at 37 mm. Deposition involved a low background pressure of O_2 ($p$$O_2$ = 5 Pa) and a substrate temperature T_{sub} = 450 °C for 10 min, after which the background gas was switched to Ar (pAr = 150 Pa), T_{sub} was increased (reaching a final temperature of 700 °C after ~30 min.) and deposition continued for a further 60 min.

The morphology and crystallinity of the as-grown samples were characterized by scanning electron microscopy (SEM, FEI Quanta 200F, equipped with an energy

dispersed X-ray (EDX) spectrometer), transmission electron microscopy (TEM, FEI, Tecnai-G2-F30), selected area electron diffraction (SAED, within the TEM system), X-ray photoelectron spectroscopy (XPS, Thermo Fisher Scientific, ESCALAB 250Xi, using an Al K_α X-ray source) and X-ray diffraction (XRD, PANalytical, X'Pert Pro, with Cu K_α radiation). PL and optical gas sensing measurements were performed using a spectrofluorometer (HORIBA, Fluoromax-4, 325 nm excitation) using a purpose-designed vacuum mini-chamber that has been described previously.[25] The required test gas concentration was provided by injecting a definite amount of H_2S. In addition to collecting the entire PL spectrum of the NR samples in different environmental gases, the spectrofluorometer was also used in 'kinetics' mode to follow the evolving emission intensity at any particular wavelength (with 1 s time resolution), thereby yielding dynamic information on the PL-based gas sensing.

3. RESULTS AND DISCUSSION

3.1 Characterization and Growth Mechanism of CuO-ZnO NRs

The morphologies of the as-grown samples were characterized by SEM, showing golden-mushroom-like motifs, with a nanoparticle capping each NR (Figure 1(a)). The NRs are randomly aligned, with diameters in the range 80-150 nm and lengths of 1-2 μm. TEM analysis (Figure 1(b)) immediately reveals that the capping nanoparticle has a much darker contrast than the shaft of the nanorod, hinting that these regions have different compositions and structures. This was explored further by SAED and XPS. SAED measurements confirm this difference, with patterns from the stem (Figure 1(c)) and cap (Figure 1(d)) conforming to, respectively, the ZnO wurtzite and CuO monoclinic crystal structures. XPS (Figure 2) confirms the presence of Cu, Zn and O and returns a Zn:Cu atomic ratio ~7.3:1, in good accord with that Zn:Cu ratio of ~6.2:1

obtained from the EDX measurements (Figure S1(a)). All of these data are consistent with formation of CuO nanoparticle capped-ZnO NRs. XRD analysis showed distinct peaks attributable to ZnO only (Figure S2(b)), which is understandable given the small size of the CuO nanoparticles and the small fraction they contribute to the total sample. As noted below, however, we conclude that Cu is also present as a dopant within the ZnO NRs.

In an effort to understand the CuO-ZnO NR formation process better, pure ZnO NRs were produced by ablating a 99.99% ZnO target under the same growth conditions. The resulting ZnO NRs were flat-topped, hexagonal in cross-section, with diameters in the range 70-180 nm and lengths of 0.5-1 μm (Figure S3), consistent with a V-S growth mechanism and with previous studies.[25] Prior reports of ZnO NRs capped by other nanoparticles formed in a PLD process assume a V-L-S growth mode,[35,38,39] wherein liquid-phase metal nanoparticles are assumed to catalyse NR growth by adsorbing reactive gas-phase species that are fed into the solid NR shafts. Well known PLD-based examples are Au nanoparticle-capped ZnO NRs, for which $T_{sub} \geq$ 800 °C is usually required in order to maintain the Au nanoparticles in the liquid phase during the NR growth process.[38,39] One previous study from our group also demonstrated V-L-S growth of ZnO NRs, catalysed in that case by Zn nanoparticles at T_{sub} = 600 °C (i.e. above the melting point of Zn, T_{mp} = 419 °C). The Zn nanoparticles were ultimately observed as oxidized ZnO capping nanoparticles.[35] Cu-catalysed V-L-S growth of ZnO nanowires has been reported previously, at temperatures around 1000 °C.[40-42] The T_{sub} used in the present work is much lower (700 °C), below the melting temperatures of both Cu (T_{mp} = 1085 °C) and CuO (T_{mp} = 1326 °C). Cu/Zn alloys with Cu:Zn ratios ≤1:4 can display $T_{mp} \leq$ 700 °C. However, the clean SAED pattern of CuO from the NR tip excludes V-L-S growth catalysed by liquid-phase Cu/Zn alloy nanoparticles as the mechanism for forming the present CuO-ZnO NRs. Further, several prior

studies suggest that the pO_2 = 5 Pa used for the first-stage deposition in this work is more than sufficient to ensure PLD growth of ZnO and CuO rather than Zn and Cu (or Cu_2O).[25,43-45] Thus the present experimental data is most rationally explained by assuming that the PLD growth of CuO-ZnO NRs follows a CuO-nanoparticle-assisted V-S-S growth mode.

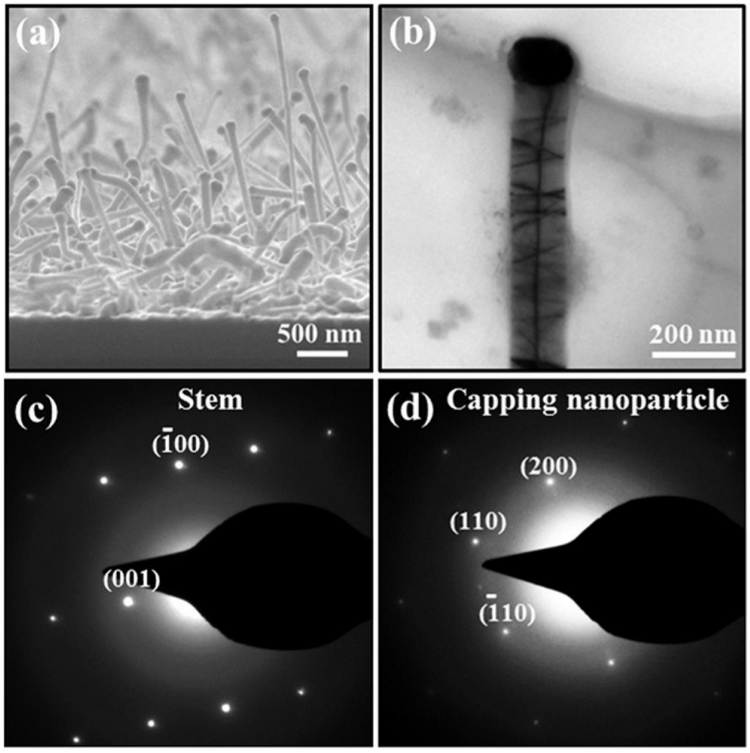

FIGURE 1. (a) SEM image of an as-grown CuO-ZnO sample; (b) TEM image of a single CuO-ZnO nanorod. SAED patterns from (c) the stem and (d) the cap of a CuO-ZnO nanorod.

As with the liquid-phase catalyst nanoparticles in conventional V-L-S growth, the solid-phase nanoparticles in a V-S-S growth mode serve both to collect material supplied from the vapour and to promote growth of a 1-dimensional solid crystal at the solid–solid interface. V-S-S mode growth of Cu-catalysed Si and Ge nanowires and of Au-catalysed ZnO and In_2O_3 nanowires have been demonstrated previously.[46-49] Most pertinent to the

present work, Tai *et al.* confirmed CuO-nanoparticle-catalysed growth of a range of oxide nanowires (MnO, Fe_3O_4, WO_3, MgO, TiO_2 and ZnO) at temperatures in the range 400-600 °C, arguing that the CuO nanoparticle acted as an intermediary, accommodating material from the vapour phase and eliminating the more noble metal (as an oxide) in the form of a NR growing from the S-S interface.[50]

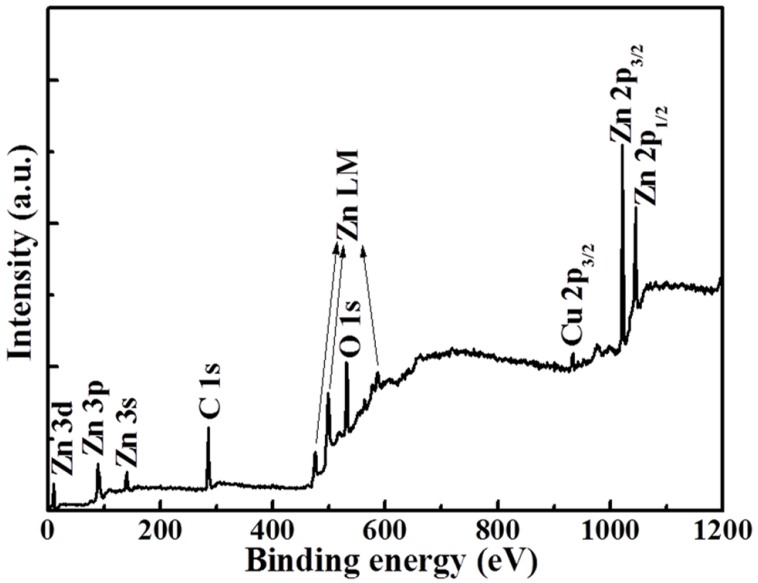

FIGURE 2. XPS data from the CuO-ZnO nanorod sample.

We speculate that the initial growth step in the present work (in pO_2 = 5 Pa at T_{sub} = 450 °C for 10 min) yields a Cu-rich oxide film that morphs into the Zn-doped CuO nanoparticles necessary for V-S-S growth as T_{sub} is raised to 700 °C. More thorough studies of the dynamics and controllability of this growth process are ongoing. For now, we simply conclude that the CuO-ZnO NRs formed in the present work demonstrate PLD of ZnO NRs via a CuO-nanoparticle-assisted V-S-S growth mode (shown in left side of Scheme 1), consistent with the expansion of the V-L-S mode for nanowire growth suggested by Samuelson and co-workers.[51]

3.2 PL of CuO-ZnO NRs

Typical PL spectra of ZnO show a sharp near-band-gap UV emission at ~380 nm and a broad visible-band emission attributed to various defects and impurities; higher ratios of these emission intensities (I_{UV}/I_{vis}) normally indicate samples of higher crystal quality.[52,53] Figure 3 compares RT-PL spectra (normalized to the same $I_{UV(max)}$) of CuO-ZnO and pure ZnO NRs. These show obvious differences: (1) the UV emission from both samples peaks at ~380 nm, but the centre of the visible band emission is shifted from ~510 nm in the case of the CuO-ZnO sample to ~530 nm for pure ZnO; (2) the I_{UV}/I_{vis} value of the former (~0.6) is very much lower than that of the latter (~33).

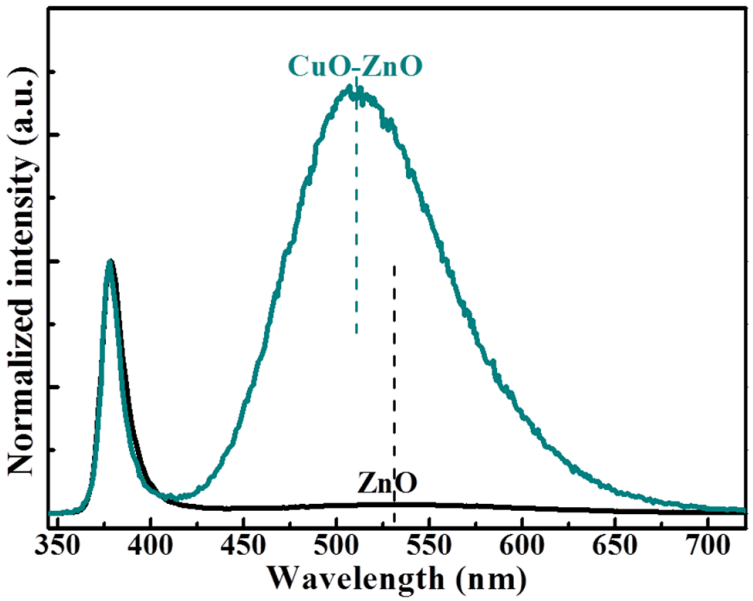

FIGURE 3. Room-temperature PL spectra of the CuO-ZnO and pure ZnO nanorod samples, with the shift in the peak of the I_{vis} component highlighted.

Our previous studies of the PL from pure ZnO NRs, of varying morphologies, consistently revealed UV emission at ~380 nm and a broad visible emission centred at ~530 nm.[25] Strong ~510 nm PL emission has been reported from Cu-doped ZnO NRs and

films, however, and assigned to the presence of dopant Cu^{2+} ions sitting at Zn sites in the ZnO lattice.[54,55] Given the small volume fraction of the capping CuO nanoparticles within the sample, it is improbable that these could account for the very different visible PL from the CuO-ZnO and pure ZnO NRs. Thus it is rational to conclude that the stem of the CuO-ZnO NR is doped with Cu.

To demonstrate this point further, Cu-doped ZnO NRs were produced by ablating a different (Cu-lean) ZnCuO target (Zn:Cu atomic ratio of 99:1) under the same growth conditions as used for the pure ZnO and the CuO-ZnO NRs. Rather than the flat-topped hexagonal NRs obtained when using pure ZnO, or the golden-mushroom-like CuO-ZnO nanorod structures, this yielded nanoneedles devoid of capping nanoparticles (as shown in the inset in Figure S4) that are reminiscent of previously reported Ni-doped ZnO nanoneedles [56] and Al-doped ZnO nanocones.[37] The PL spectrum of these Cu-doped ZnO NRs (Figure S4) shows a ~380 nm UV emission peak and a ~510 nm visible emission band that matches well with the CuO-ZnO results. The I_{UV}/I_{vis} ratio in the case of the Cu-doped ZnO NRs (~5.6) is intermediate between those found for the pure ZnO and the CuO-ZnO NRs, suggesting that the Cu concentration in the stem of the latter is higher than in these Cu-doped ZnO NRs.

3.3 H_2S Sensing Properties of CuO-ZnO NRs

The H_2S sensing properties of the as-grown CuO-ZnO nanorod samples were examined by monitoring their PL spectra at RT. Figure 4 shows RT-PL spectra measured sequentially in air at atmospheric pressure, in air+15 ppm H_2S, and then again in air. I_{UV} at 380 nm is significantly increased in the presence of 15 ppm H_2S, while I_{vis} at 510 nm decreases slightly. The original profile of the PL spectrum was restored once the

environmental gas reverted to air. Again, for comparison, the PL spectra of the pure and Cu doped-ZnO nanorod samples were also traced through the same environmental gas cycle. The PL spectrum of the former was essentially unchanged when exposed to 15 ppm H_2S in air while, in the case of the Cu doped-ZnO nanorod sample, I_{UV} showed a ~28% increase but, again, the visible emission barely changed (Figures S5 and S6).

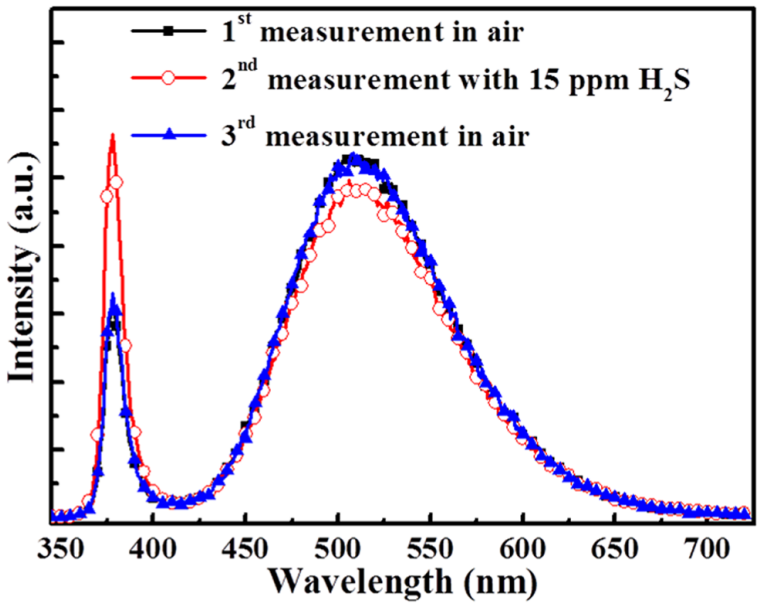

FIGURE 4. Room-temperature PL spectra of the CuO-ZnO nanorods measured sequentially in air, in air+15 ppm H_2S, and then again in air.

We define the PL-based H_2S sensing response R as

$$R\% = (I_g - I_a)/I_a \times 100\% \qquad (1)$$

where I_a and I_g are, respectively, the $I_{UV(max)}$ measured in air and in the test gas. R for the CuO-ZnO NRs in the presence of 15 ppm H_2S is ~78, much higher than that of the pure ZnO (R~5, Figure S5) or the Cu-doped ZnO NRs (R ~28, Figure S6), confirming the superior H_2S sensing performance of CuO-ZnO NRs compared with the pure ZnO and Cu-doped ZnO NRs produced in this work.

Time dependent measurements of I_{UV} from the CuO-ZnO NRs upon exposure to different concentrations of H_2S in the range 0.5-15 ppm (Figure 5) serve to illustrate the pronounced response of this sample down to 0.5 ppm H_2S (at which point R is still ~25) and that R scales with the H_2S concentration. The absolute value of $I_{UV(max)}$ recovers well upon re-exposing the CuO-ZnO NR sample to air. The response and recovery times estimated from Figure 5 are, respectively ~3 min and ~15 s, both of which are shorter than the majority of reported electrical H_2S sensors when operating at RT.[8,11-13,15] Moreover, as shown in Figure S7, PL-based sensing with the CuO-ZnO NR sample shows a high selectivity towards H_2S.

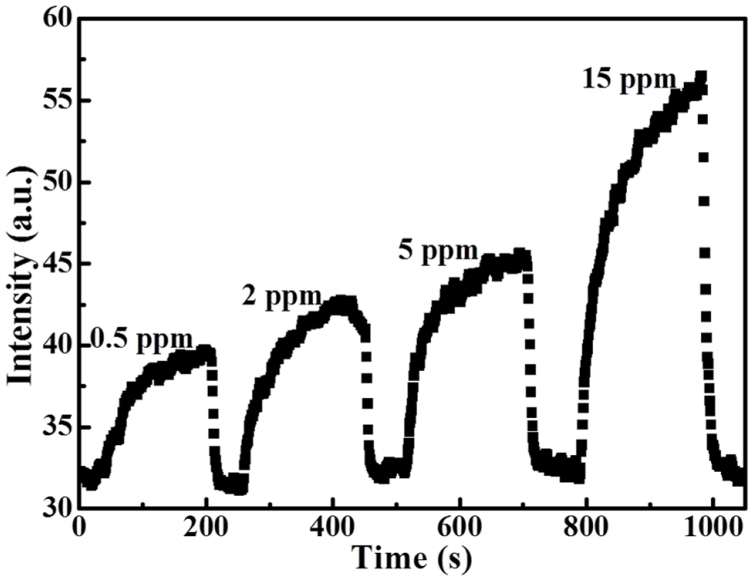

FIGURE 5. Dynamic I_{UV} response of CuO-ZnO nanorods upon exposure to 0.5-15 ppm H_2S in air samples at RT.

3.4 H_2S Sensing Mechanisms of CuO-ZnO NRs

To develop an understanding of the PL-based H_2S sensing properties of CuO-ZnO NRs, we start by summarising proposed mechanisms for the electrical sensing of H_2S using

pure ZnO, Cu-doped ZnO, and CuO-ZnO heterostructures. In the case of pure ZnO samples, adsorbed oxygen species like O^{2-}, O^{-} and O_2^{-} have been suggested to play key roles,[6,12] extracting electrons and thereby forming an electron depletion layer on the surface and reducing the electrical conductivity. By reacting with these adsorbed oxygen species, H_2S causes these trapped electrons to be released back to the ZnO sample, reducing the thickness of the depletion layer and thus enhancing the sample conductivity. Given that O_2^{-} is the dominant adsorbed oxygen species on a ZnO surface at temperatures below 100 °C,[12] the electrical sensing of H_2S by ZnO at RT can be expressed in terms of the following reaction:

$$2H_2S(g) + 3O_2^{-}(ad) \leftrightarrow 2H_2O(g) + 2SO_2(g) + 3e^{-} \qquad (2)$$

Both the surface area to volume (S/V) ratio and the density of active sites for gas adsorption on the ZnO surface are considered to be important in determining the sensitivity of the sensor. Besides controlling the surface morphology,[6,11,57] Cu doping has also been confirmed as an effective strategy for improving the H_2S electrical sensing properties of ZnO by providing more active sites (*e.g.* oxygen vacancies) for gas adsorption.[20] Conversely, several groups have also suggested that ZnO and CuO can be sulfurized by H_2S, yielding semiconducting ZnS [5,18] and metallic CuS,[13,21-23] and that these sulfides can then convert back to the corresponding oxides when exposed to ambient oxygen via desulfurization reactions,[5,21-23,58] even at RT.[13] Formation of ZnS on the surface of ZnO could reduce the trapping of electrons by adsorbed oxygen and thus enhance the conductivity. Notably, in the case of CuO-ZnO heterostructures, formation of metallic CuS not only directly enhances their conductivity, but also releases trapped electrons from the CuO-ZnO *p*-*n* junctions to ZnO, thereby increasing the conductivity of

the ZnO. On this basis, therefore, the much improved electrical sensing of H_2S by CuO-ZnO heterostructures (*cf*. pure ZnO) could be attributed to the sulfurization of CuO.[13,21-23]

In addition to enhancing the conductivity, the release of trapped electrons to the ZnO can also impact on its PL properties. The UV emission is generally considered to emanate from the inner part of the NRs, beneath the depletion layer.[25,59] I_{UV} will therefore be sensitively dependent on any expansion or reduction of the depletion layer. Previous demonstrations of I_{UV}-based sensing of O_2 and NO_2 by pure ZnO NRs [25,29] have been rationalised using such a picture of trapping and release of electrons (and the concomitant expansion and reduction of the depletion layer) as a result of gas adsorption/desorption. Such a mechanism is also consistent with the present I_{UV}-based sensing of H_2S by CuO-ZnO NRs, as illustrated schematically in the right side of Scheme 1. As with the electrical sensing mechanisms, reactions of H_2S with adsorbed O_2^- and with ZnO reduce the thickness of the depletion layer and thus enhance I_{UV} from both CuO-ZnO and pure ZnO NRs. More importantly, in the present context, both the Cu-doped ZnO stems and the CuO capping nanoparticles can contribute to the enhanced I_{UV}-based H_2S sensing properties of CuO-ZnO NRs (cf. with pure ZnO NRs). Given the relatively low activities of sulfurization and desulfurization reactions at RT and the relatively fast measured response and recovery times, we suggest that Cu doping plays a more important role than the CuO nanoparticles in the H_2S sensing performance of CuO-ZnO NRs.

Apart from enhancing the UV emission of CuO-ZnO, Cu-doped ZnO and pure ZnO NRs (to differing extents), H_2S adsorption can also influence I_{vis}. H_2S-induced release of electrons trapped at the sample surface into the bulk might be expected to cause an increase in I_{vis} originating from bulk defects, whereas any H_2S induced reduction in the

number of adsorbed oxygen species and Cu^{2+} dopants on the ZnO surface will tend to reduce I_{vis}. The relative efficiencies of these competing effects would almost certainly be sample dependent and hard to predict. For all these reasons, the sharp, strong and sensitive UV emission offers overwhelming advantages (*cf.* the visible emission) as the indicator for H_2S sensing.

The CuO-ZnO NRs have much smaller average diameters (estimated as ~110 nm) than the Cu-doped ZnO NRs (which have root diameters ~300 nm) and thus much larger S/V ratios. Thus it is reasonable that *R* for the CuO-ZnO NRs is roughly twice that for the Cu-doped ZnO NRs (in the presence of 15 ppm H_2S). The average diameter of the pure ZnO NRs (~120 nm) is similar to that of the CuO-ZnO NRs, yet the response of the former to 15 ppm of H_2S is only ~1/15 as large. The much higher response of the CuO-ZnO NRs is attributed to Cu doping of the stems and the capping CuO nanoparticles, while the high selectivity of the CuO-ZnO NRs to H_2S is ascribed to the higher RT reactivity of this gas [11,12] relative to the other conventional gases tested in this work.

■ CONCLUSIONS

Novel CuO nanoparticle-capped ZnO NRs have been produced by a PLD method. These NRs grow via a V-S-S mode, with CuO nanoparticles acting as the catalyst. The Cu-doped ZnO stem and the CuO capping nanoparticles afford excellent optical sensing properties towards H_2S at RT, with a demonstrated sensitivity down to sub-ppm concentrations and a high selectivity. This work provides a first demonstration of a PL-based H_2S gas sensor, and also suggests the feasibility of using CuO nanoparticles to catalyse growth of ZnO NRs via a V-S-S mode using gas phase methods other than PLD.

■ ASSOCIATED CONTENT

Supporting Information Available: EDX spectra of CuO-ZnO and Cu-doped ZnO nanorods, XRD patterns of pure ZnO nanorods and CuO-ZnO nanorods, SEM images of pure ZnO nanorods, PL and SEM image of Cu-doped ZnO nanorods, PL spectra of the pure and Cu-doped ZnO nanorods measured sequentially in air, in air+15 ppm H_2S, and in air again, and gas selectivity of CuO-ZnO nanorods. This material is available free of charge via the Internet at http://pubs.acs.org.

■ AUTHOR INFORMATION

Corresponding authors

*E-mail: sunye@hit.edu.cn, miaoyu_che@hit.edu.cn, mike.ashfold@bristol.ac.uk

Author Contributions

X.L. and B.D. were responsible for sample preparation and gas sensing measurements. Y.S., M.Y. and M.N.R.A. conceived and designed the experiments, helped in the data discussion and interpretation, and were the main authors of the article. Y.Y., W.T., C.C. and L.S. contributed sample characterization and data interpretation. B.Y. and W.C. assisted with preparing the ZnCuO targets and the PLD samples.

■ ACKNOWLEDGMENT

This work is financially supported by the National Basic Research Program of China (973 Program, Grant No. 2013CB632900), the National Natural Science Foundation of China (Grant Nos. 11104046, 21473045 and 51401066) and by Fundamental Research Funds from the Central

University (Grant Nos. HIT.BRETIII.201216, HIT.BRETIII.201225, HIT.BRE TIV.201313 and PIRS OF HIT A201503).

■ REFERENCES

(1) Guo, Z.; Chen, G.; Zeng, G.; Liu, L.; Zhang, C. Metal Oxides and Metal Salt Nanostructures for Hydrogen Sulfide Sensing: Mechanism and Sensing Performance *RSC Adv.* **2015**, 5, 54793-54805.

(2) Li, Y.; Luo, W.; Qin, N.; Dong, J.; Wei, J.; Li, W.; Feng, S.; Chen, J.; Xu, J.; Elzatahry, A. A.; Es-Saheb, M. H.; Deng Y.; Zhao, D. Highly Ordered Mesoporous Tungsten Oxides with a Large Pore Size and Crystalline Framework for H_2S Sensing *Angew. Chem. Int. Ed*. **2014**, 53, 9035-9040.

(3) Wan, X.; Wang, J.; Zhu L.; Tang, J. Gas Sensing Properties of Cu_2O and Its Particle Size and Morphology-Dependent Gas-Detection Sensitivity *J. Mater. Chem. A* **2014**, 2, 13641-13647.

(4) Datta, N.; Ramgir, N. S.; Kumar, S.; Veerender, P.; Kaur, M.; Kailasaganapathi, S.; Debnath, A. K.; Aswal D. K.; Gupta, S. K. Role of Various Interfaces of CuO/ZnO Random Nanowire Networks in H_2S Sensing: An Impedance and Kelvin Probe Analysis *Sens. Actuators, B* **2014**, 202, 1270-1280.

(5) Huang, H.; Xu, P.; Zheng, D.; Chen C.; Li, X. Sulfuration–Desulfuration Reaction Sensing Effect of Intrinsic ZnO Nanowires for High-Performance H_2S Detection *J. Mater. Chem. A* **2015**, 3, 6330-6339.

(6) Diao, K.; Zhou, M.; Zhang, J.; Tang, Y.; Wang S.; Cui, X. High Response to H_2S Gas with Facile Synthesized Hierarchical ZnO Microstructures *Sens. Actuators, B* **2015**, 219, 30-37.

(7) Chen, Y.; Meng, F.; Yu, H.; Zhu, C.; Wang, T.; Gao P.; Ouyang, Q. Sonochemical Synthesis and ppb H_2S Sensing Performances of CuO Nanobelts *Sens. Actuators, B* **2013**, 176, 15-21.

(8) Zhou, L.; Shen, F.; Tian, X.; Wang, D.; Zhang, T.; Chen, W. Stable Cu_2O Nanocrystals Grown on Functionalized Graphene Sheets and Room Temperature H_2S Gas Sensing with Ultrahigh Sensitivity *Nanoscale* **2013**, 5, 1564-1569.

(9) Mei, L.; Chen, Y.; Ma, J. Gas Sensing of SnO_2 Nanocrystals Revisited: Developing Ultra-Sensitive Sensors for Detecting the H_2S Leakage of Biogas *Sci. Rep.* **2014**, 4, 6028.

(10) Deng, J.; Ma, J.; Mei, L.; Tang, Y.; Chen, Y.; Lv, T.; Xu, Z.; Wang, T. Porous α-Fe_2O_3 Nanosphere-based H_2S Sensor with Fast Response, High Selectivity and Enhanced Sensitivity *J. Mater. Chem. A* **2013**, 1, 12400-12403.

(11) Hosseini, Z. S.; Irajizad, A.; Mortezaali, A. Room Temperature H_2S Gas Sensor based on Rather Aligned ZnO Nanorods with Flower-Like Structures *Sens. Actuators, B* **2015**, 207, 865-871.

(12) Ramgir, N. S.; Sharma, P. K.; Datta, N.; Kaur, M.; Debnath, A. K.; Aswal, D. K.; Gupta, S. K. Room Temperature H_2S Sensor based on Au Modified ZnO Nanowires *Sens. Actuators, B* **2013**, 186, 718-726.

(13) Kaur, M.; Ganapathi, K.; Mukund, V.; Jain, C.; Ramgir, N. S.; Datta, N.; Bhattacharya, S.; Debnath, A. K.; Aswal, D. K.; Gupta, S. K. Selective H_2S Detection by CuO Functionalized ZnO Nanotetrapods at Room Temperature *Mater. Chem. Phys.* **2014**, 143, 1319-1324.

(14) Zhang, S.; Zhang, P.; Wang, Y.; Ma, Y.; Zhong, J.; Sun, X. Facile Fabrication of a Well-Ordered Porous Cu-Doped SnO_2 Thin Film for H_2S Sensing *ACS Appl. Mater. Interfaces* **2014**, 6, 14975-14980.

(15) Ma, J.; Liu, Y.; Zhang, H.; Ai, P.; Gong, N.; Wu, Y.; Yu, D. Room Temperature ppb Level H_2S Detection of a Single Sb-doped SnO_2 Nanoribbon Device *Sens. Actuators, B* **2015**, 216, 72-79.

(16) Woo, H.-S.; Kwak, C.-H.; Kim, I.-D.; Lee, J.-H. Selective, Sensitive, and Reversible Detection of H_2S using Mo-Doped ZnO Nanowire Network Sensors *J. Mater. Chem. A* **2014**, 2, 6412-6418.

(17) Sun, G.-J.; Choi, S.-W.; Katoch, A.; Wu, P.; Kim, S. S. Bi-Functional Mechanism of H_2S Detection using CuO–SnO_2 Nanowires *J. Mater. Chem. C* **2013**, 1, 5454-5462.

(18) Qi, G.; Zhang, L.; Yuan, Z. Improved H_2S Gas Sensing Properties of ZnO Nanorods Decorated by a Several nm ZnS Thin Layer *Phys. Chem. Chem. Phys.* **2014**, 16, 13434-13439.

(19) Yoon, J.-W.; Hong, Y. J.; Kang, Y. C.; Lee, J.-H. High Performance Chemiresistive H_2S Sensors using Ag-Loaded SnO_2 Yolk–Shell Nanostructures *RSC Adv.* **2014**, 4, 16067-16074.

(20) Zhao, M.; Wang, X.; Ning, L.; Jia, J.; Li, X.; Cao, L. Electrospun Cu-doped ZnO Nanofibers for H_2S Sensing *Sens. Actuators, B* **2011**, 156, 588-592.

(21) Katoch, A.; Choi, S.-W.; Kim, J.-H.; Lee, J. H.; Lee, J.-S.; Kim, S. S. Importance of the Nanograin Size on the H_2S-Sensing Properties of ZnO–CuO Composite Nanofibers *Sens. Actuators, B* **2015**, 214, 111-116.

(22) Kim, J.; Kim, W.; Yong, K. CuO/ZnO Heterostructured Nanorods: Photochemical Synthesis and the Mechanism of H_2S Gas Sensing *J. Phys. Chem. C* **2012**, 116, 15682-15691.

(23) Xu, Z.; Duan, G.; Li, Y.; Liu, G.; Zhang, H.; Dai, Z.; Cai, W. CuO–ZnO Micro/Nanoporous Array-Film-based Chemosensors: New Sensing Properties to H_2S *Chem. Eur. J.* **2014**, 20, 6040-6046.

(24) Kadir, R. A.; Rani, R. A.; Alsaif, M. M. Y. A.; Ou, J. Z.; Wlodarski, W.; O'Mullane, A. P.; Kalantar-Zadeh, K. Optical Gas Sensing Properties of Nanoporous Nb_2O_5 Films *ACS Appl. Mater. Interfaces* **2015**, 7, 4751-4758.

(25) Liu, X.; Sun, Y.; Yu, M.; Yin, Y.; Yang, B.; Cao, W.; Ashfold, M. N. R. Incident Fluence

Dependent Morphologies, Photoluminescence and Optical Oxygen Sensing Properties of ZnO Nanorods Grown by Pulsed Laser Deposition *J. Mater. Chem. C* **2015**, 3, 2557-2562.

(26) Tabassum, R.; Mishra, S. K.; Gupta, B. D. Surface Plasmon Resonance-Based Fiber Optic Hydrogen Sulphide Gas Sensor Utilizing Cu–ZnO Thin Films *Phys. Chem. Chem. Phys.* **2013**, 15, 11868-11874.

(27) Petruci, J. F. da S.; Fortes, P. R.; Kokoric, V.; Wilk, A.; Raimundo, Jr., I. M.; Cardoso, A. A.; Mizaikoff, B. Monitoring of Hydrogen Sulfide via Substrate-Integrated Hollow Waveguide Mid-Infrared Sensors in Real-Time *Analyst* **2014**, 139, 198-203.

(28) Sanchez-Valencia, J. R.; Alcaire, M.; Romero-Gómez, P.; Macias-Montero, M.; Aparicio, F. J.; Borras, A.; Gonzalez-Elipe, A. R.; Barranco, A. Oxygen Optical Sensing in Gas and Liquids with Nanostructured ZnO Thin Films Based on Exciton Emission Detection *J. Phys. Chem. C* **2014**, 118, 9852-9859.

(29) Cretì, A.; Valerini, D.; Taurino, A.; Quaranta, F.; Lomascolo M.; Rella, R. Photoluminescence Quenching Processes by NO_2 Adsorption in ZnO Nanostructured Films *J. Appl. Phys.* **2012**, 111, 073520.

(30) Aad, R.; Simic, V.; Cunff, L. L.; Rocha, L.; Sallet, V.; Sartel, C.; Lusson, A.; Couteau, C.; Lerondel, G. ZnO Nanowires as Effective Luminescent Sensing Materials for Nitroaromatic Derivatives *Nanoscale* **2013**, 5, 9176-9180.

(31) Lee, S. K.; Son, J. Y. Epitaxial Growth of Thin Films and Nanodots of ZnO on Si(111) by Pulsed Laser Deposition *Appl. Phys. Lett.* **2012**, 100, 132109.

(32) Sun, Y.; Fuge, G. M.; Ashfold, M. N. R. Growth of Aligned ZnO Nanorod Arrays by Catalyst-Free Pulsed Laser Deposition Methods *Chem. Phys. Lett.* **2004**, 396, 21-26.

(33) Sun, Y.; Ashfold, M. N. R. Photoluminescence from Diameter-Selected ZnO Nanorod

Arrays *Nanotechnology* **2007**, 18, 245701.

(34) Ghosh, S.; Khan, G. G.; Varma S.; Mandal, K. Influence of Film Thickness and Oxygen Partial Pressure on Cation-Defect-Induced Intrinsic Ferromagnetic Behavior in Luminescent p-Type Na-Doped ZnO Thin Films *ACS Appl. Mater. Interfaces* **2013**, 5, 2455-2461.

(35) Sun, Y.; Fuge, G. M.; Ashfold, M. N. R. Growth Mechanisms for ZnO Nanorods Formed by Pulsed Laser Deposition *Superlattices Microstruct.* **2006**, 39, 33-40.

(36) Sun, Y.; Doherty, R. P.; Warren, J. L.; Ashfold, M. N. R. Effect of Incident Fluence on the Growth of ZnO Nanorods by Pulsed Excimer Laser Deposition *Chem. Phys. Lett.* **2007**, 447, 257-262.

(37) Sun, Y.; Addison, K. E.; Ashfold, M. N. R. Growth of Arrays of Al-Doped ZnO Nanocones by Pulsed Laser Deposition *Nanotechnology* **2007**, 18, 495601.

(38) Marcu, A.; Trupina, L.; Zamanid, R.; Arbiol, J.; Grigoriu, C.; Morante, J. R. Catalyst Size Limitation in Vapor–Liquid–Solid ZnO Nanowire Growth using Pulsed Laser Deposition *Thin Solid Films* **2012**, 520, 4626-4631.

(39) Weigand, C.; Tveit, J.; Ladam, C.; Holmestad, R.; Grepstad, J.; Weman, H. Epitaxial Relationships of ZnO Nanostructures Grown by Au-Assisted Pulsed Laser Deposition on *c*- and *a*-Plane Sapphire *J. Cryst. Growth* **2012**, 355, 52-58.

(40) Eustis, S.; Meier, D. C.; Beversluis, M. R.; Nikoobakht, B. Analysis of Copper Incorporation into Zinc Oxide Nanowires *ACS Nano* **2008**, 2, 368-376.

(41) Zhao, Y. M.; Li, Y. H.; Jin, Y. Z.; Zhang, X. P.; Hu, W. B.; Ahmad, I.; McCartney, G.; Zhu, Y. Q. Growth and Characterization of Cu-Catalyzed ZnO Nanowires *J. Phys.: Conf. Ser.* **2007**, 61, 703-707.

(42) Li, S. Y.; Lee, C. Y.; Tseng, T. Y. Copper-Catalyzed ZnO Nanowires on Silicon (100) Grown

by Vapor–Liquid–Solid Process *J. Cryst. Growth* **2003**, 247, 357-362.

(43) Zhu, B. L.; Zhao, X. Z.; Xu, S.; Su, F. H.; Li, G. H.; Wu, X. G.; Wu, J.; Wu R.; Liu, J. Oxygen Pressure Dependences of Structure and Properties of ZnO Films Deposited on Amorphous Glass Substrates by Pulsed Laser Deposition *Jpn. J. Appl. Phys.* **2008**, 47, 2225-2229.

(44) Kawwam, M.; Alharbi, F.; Aldwayyan, A.; Lebbou, K. Morphological Study of PLD Grown CuO Films on $SrTiO_3$, Sapphire, Quartz and MgO Substrates *Appl. Surf. Sci.* **2012**, 258. 9949-9953.

(45) Chen, A.; Long, H.; Li, X.; Li, Y.; Yang, G.; Lu, P. Controlled Growth and Characteristics of Single-Phase Cu_2O and CuO Films by Pulsed Laser Deposition *Vacuum* **2009**, 83, 927-930.

(46) Richards, B. T.; Gaskey, B.; Levin, B. D. A.; Whitham, K.; Muller, D.; Hanrath, T. Direct Growth of Germanium and Silicon Nanowires on Metal Films *J. Mater. Chem. C* **2014**, 2, 1869-1878.

(47) Wen, C.-Y.; Reuter, M. C.; Tersoff, J.; Stach, E. A.; Ross, F. M. Structure, Growth Kinetics, and Ledge Flow during Vapor-Solid-Solid Growth of Copper-Catalyzed Silicon Nanowires *Nano Lett.* **2010**, 10, 514-519.

(48) Kim, B. J.; Kim, M. W.; Jang, J. S.; Stach, E. A. Real Time Observation of ZnO Nanostructure Formation via the Solid–Vapor and Solid–Solid–Vapor Mechanisms *Nanoscale* **2014**, 6, 6984-6990.

(49) Barth, S.; Seifner, M. S.; Bernardi, J. Growth of Monocrystalline In_2O_3 Nanowires by a Seed Orientation Dependent Vapour–Solid–Solid Mechanism *J. Mater. Chem. C* **2014**, 2, 5747-5751.

(50) Tai, K.; Sun, K.; Huang, B.; Dillon, S. J. Catalyzed Oxidation for Nanowire Growth

Nanotechnology **2014**, 25, 145603.

(51) Wacaser, B. A.; Dick, K. A.; Johansson, J.; Borgström, M. T.; Deppert K.; Samuelson, L. Preferential Interface Nucleation: An Expansion of the VLS Growth Mechanism for Nanowires *Adv. Mater*. **2009**, 21, 153-165.

(52) Yin, Y.; Sun, Y.; Yu, M.; Liu, X.; Yang, B.; Liu, D.; Liu, S.; Cao W.; Ashfold, M. N. R. Arrays of Nanorods Composed of ZnO Nanodots Exhibiting Enhanced UV Emission and Stability *Nanoscale* **2014**, 6, 10746-10751.

(53) Yin, Y.; Sun, Y.; Yu, M.; Liu, X.; Yang, B.; Liu, D.; Liu, S.; Cao. W.; Ashfold, M. N. R. Reagent Concentration Dependent Variations in the Stability and Photoluminescence of Silica-Coated ZnO Nanorods *Inorg. Chem. Front.* **2015**, 2, 28-34.

(54) Huang, X. H.; Zhang, C.; Tay, C. B.; Venkatesan, T.; Chua, S. J. Green Luminescence from Cu-Doped ZnO Nanorods: Role of Zn Vacancies and Negative Thermal Quenching *Appl. Phys. Lett*. **2013**, 102, 111106.

(55) Khan, Z. A.; Rai, A.; Barman, S. R.; Ghosh, S. Green Luminescence and Room Temperature Ferromagnetism in Cu Doped ZnO *Appl. Phys. Lett.* **2013**, 102, 022105.

(56) Singh, S.; Nakamura, D.; Sakai, K.; Okada T.; Rao, M. S. R. Investigation of Low-Temperature Excitonic and Defect Emission from Ni-Doped ZnO Nanoneedles and V-Doped ZnO Nanostructured Film *New J. Phys.* **2010**, 12, 023007.

(57) Iversen, K. J.; Spencer, M. J. S. Effect of ZnO Nanostructure Morphology on the Sensing of H_2S Gas *J. Phys. Chem. C* **2013**, 117, 26106-26118.

(58) Park, S.; Kim, S.; Kheel, H.; Hyun, S. K.; Jin, C.; Lee, C. Enhanced H_2S Gas Sensing Performance of Networked CuO-ZnO Composite Nanoparticle Sensor *Mater. Res. Bull.* **2016**, http://dx.doi.org/10.1016/j.materresbull.2016.02.011.

(59) Sun, Y.; Ndifor-Angwafor, N. G.; Riley D. J.; Ashfold, M. N. R. Synthesis and Photoluminescence of Ultra-Thin ZnO Nanowire/Nanotube Arrays Formed by Hydrothermal Growth *Chem. Phys. Lett.* **2006**, 431, 352-357.

Abstract Graphic

Sensitive Room Temperature Photoluminescence-based Sensing of H_2S with Novel CuO-ZnO Nanorods

Xiao Liu, Baosheng Du, Ye Sun, Miao Yu,* Yongqi Yin, Wei Tang, Chong Chen, Lei Sun, Bin Yang, Wenwu Cao, and Michael N. R. Ashfold**